Rugotaxis: Droplet motion without external energy supply

PANAGIOTIS E. THEODORAKIS[1], SERGEI A. EGOROV[2,3,4] and ANDREY MILCHEV[5]

[1] *Institute of Physics, Polish Academy of Sciences, Al. Lotników 32/46, 02-668 Warsaw, Poland*
[2] *Department of Chemistry, University of Virginia, Charlottesville, VA 22901, USA*
[3] *Institut für Physik, Johannes Gutenberg Universität Mainz, 55099 Mainz, Germany*
[4] *Leibniz-Institut für Polymerforschung, Institut Theorie der Polymere, Hohe Str. 6, 01069 Dresden, Germany*
[5] *Bulgarian Academy of Sciences, Institute of Physical Chemistry, 1113 Sofia, Bulgaria*

Abstract – Nano-patterned substrates offer possibilities for controlling the motion of fluids without external energy supply in novel technologies in microfluidics, coatings, *etc.* Here, we report on the rugotaxial motion of droplets on wrinkled substrates with gradient in the wavelength of the wrinkles by exploring a broad range of parameters, such as amplitude of the wrinkles, substrate wettability, droplet size and wavelength gradient. Adopting a theoretical and molecular dynamics approach, we determine the Cassie–Baxter and Wenzel states of the droplets, investigate the efficiency of rugotaxis as a function of different parameters, and discuss additional effects, such as pinning. We find that shallow wrinkles characterised by small wavelength gradients, and moderate adhesion of the droplet to the substrate favour the rugotaxis motion with growing droplet size, when pinning is avoided. We also find that the driving force in rugotaxis is the gain in interfacial energy between the droplet and the substrate as the droplet enters regions of denser wrinkles (smaller wavelengths of the wrinkles).

The development of various technologies in microfluidics, microfabrication, coatings, and biology require the motion of fluids along predetermined trajectories [1–8]. A possibility of realising such motion is by using *gradient* substrates, namely substrates with gradually changing properties in a certain direction along the substrate [9–12]. For example, by exploiting differences in tissue stiffness, cells are able to move from softer to stiffer regions, a phenomenon known as durotaxis [13,14]. Durotaxis is particularly appealing for nanotechnology applications, because fluid motion is sustainable without providing external energy from a source [15–18]. In contrast, motion caused, for example, by a temperature gradient (thermotaxis) would require external energy supply into the system to maintain the gradient that is responsible for the fluid motion [19]. In this regard,characteristic cases of droplet motion caused by external energy supply are chemically driven droplets [20,21], and droplets on vibrated substrates [22–24] or wettability ratchets [25–27]. Moreover, in the case of vibrated substrates, the vibrations allow the droplet to overcome pinning and move against its gravity, as a consequence of an up or down symmetry breaking caused by the substrate that cause the deformation of the droplet [22–24].

Hiltl and Böker have recently demonstrated in their experiments the possibility of causing the motion of a water droplet onto a sinusoidal wrinkle-patterned, solid substrate without using an external energy source, a phenomenon known as rugotaxis [28]. In this case, the wavelength characterising the wavy shape of the wrinkles decays as a function of the position, namely, there is a wavelength gradient characterising the wrinkles [28]. Hiltl and Böker have found that the droplet moves toward smaller wrinkle dimensions (wrinkles described by smaller wavelength). By investigating wrinkled substrates with wavelengths between 230 and 1200 nm, and amplitudes ranging from 7 to 230 nm, they attributed this phenomenon to the imbalance of the receding and advancing contact angles. In particular, contact angles correlate with the wavelength of the wrinkles, that is, larger contact angles for larger wavelengths, which naturally corresponds to differences of the substrate density along the direction of the wavelength gradient and the rugotaxial motion. The imbalance
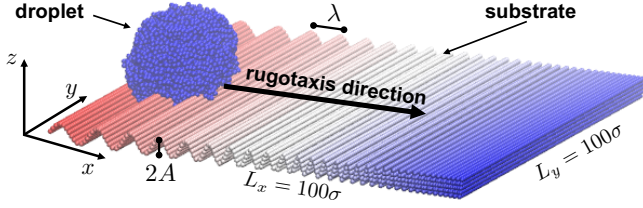
Fig. 1: A typical snapshot of an initial configuration for the rugotaxis study with a droplet on a wrinkled substrate with gradient in the wavelength, λ, characterising the sinusoidal shape of the wrinkles. The dimensions of the substrate in the x and y directions are $L_x = L_y = 100\sigma$. The amplitude of the wrinkles is $A = 2\sigma$, the initial wavelength at the very left side of the substrate is $\lambda_0 = 10\sigma$ and that at the right side of the substrate is $\lambda_E = \sigma$. Given the linear decrease of the wavelength in the x direction, the wavelength gradient is constant and equal to $G_\lambda = (\lambda_0 - \lambda_E)/L_x = 0.09$, in this case. The rugotaxial motion of the droplet takes place in the x direction, along the wavelength gradient, as indicated by an arrow. Snapshots have been produced using VMD software [50].

between the advancing and the receding contact angles as the driving force for droplet motion has been theoretically discussed in detail by Brochard [29] in the context of chemical or thermal gradients. Moreover, more recently, an asymptotic theory has been developed to match the advancing and the receding side to respective solutions of the problem at the microscale, where the velocity at the microscale is used as the small parameter of an asymptotic expansion, which provides the droplet shape and its velocity as a function of the wettability gradient [30].

While wrinkled substrates without gradients [31–38] and substrates of similar geometries [39–45] have been studied in different contexts, rugotaxis have remained unexplored. Inspired by the work of Hiltl and Böker [28], we employ theoretical [46, 47] and molecular dynamics (MD) [17] modelling to investigate the self-propelled motion of nanodroplets on wrinkled, solid substrates with wavelength gradient characterising the wrinkles. We show that the efficiency depends on the particular choice of parameters for the substrate, which leads to specific scenarios, when rugotaxis is possible. We also find that the driving force of the rugotaxis phenomenon is the gain in the interfacial energy between the droplet and the substrate as the droplet reaches areas of denser wrinkles. Toward studying rugotaxis, we have also explored the transition between Cassie–Baxter [48] (CB, state where the liquid droplet does not penetrate the grooves on rough surfaces and leaves air gaps between the droplet and the substrate) and Wenzel [49] (W, state where the droplet penetrates the grooves without any gap between the droplet and the substrate despite its roughness) states in substrates without gradient and compared our results with theoretical predictions [38] in order to set the stage for a better understanding of rugotaxis.

Figure 1 illustrates an initial configuration of our *in silico* experiments for a particular case. A liquid droplet is placed on a sinusoidal substrate with wavelength gradient of the wrinkles in the x direction. This requires that the x and z coordinates of the beads be associated with the relation $z = A \sin(2\pi x/\lambda)$, where A is the amplitude and λ is the wavelength characterising the wrinkles. To implement a gradient in the wavelength of the wrinkles, one needs to multiply the wavelength with a coefficient that depends linearly on the position x of the bead on the substrate. Such substrate design is able to cause the rugotaxial motion of the droplet in the x direction along the wavelength gradient. Rugotaxial motion will take place for a particular set of parameters characterising the substrate design, such as the amplitude of the wrinkles, A, as well as the initial wavelength, λ_0 at the one end of the substrate and the final wavelength at the other end, λ_E ($\lambda_0 > \lambda_E$). The latter wavelengths determine the wavelength gradient of the wrinkles, expressed as $G_\lambda = (\lambda_0 - \lambda_E)/L_x$ (L_x is the linear dimension of the substrate in the x direction). The adhesion of the droplet to the substrate is controlled through the ε_{sp} parameter of the Lennard-Jones potential. The details of our MD model are the same as in Ref. [17] (See Supplmentary Information). In order to suppress droplet evaporation, we consider polymer melt droplets made of sufficiently long linear macromolecules of length $N = 10$ monomers each. This choice ensures the absence of evaporation effects, which might have otherwise affected the outcome of our *in silico* experiments [17]. In our study, different droplet sizes were considered, namely $N_p = 100$, 600, and 4800, where N_p is the total number of polymer chains comprising the droplet.

By investigating a range of amplitudes ($A = 0.5$–2.5σ), wavelengths ($\lambda = 1$–10σ) and strengths of attraction ($\varepsilon_{sp} = 0.1$–0.7ε) between the droplet and the substrate, we have initially determined the state [*e.g.* Wenzel (W), Cassie–Baxter (CB)] of the droplet on substrates *without gradient* by using MD simulation. Our results are presented in the form of state diagrams in Fig. 2 for two cases, namely $A = \sigma$ and $A = 2\sigma$. The cases $\lambda = \sigma$ are not shown in the figure, because they represent flat substrates and a discussion about W and CB states would be irrelevant. Also, cases that the attraction strength $\varepsilon_{sp} = 0.1\varepsilon$ were omitted, because the droplet would detach from the substrate due to its thermal fluctuations. The results of Fig. 2 are in agreement with theoretical predictions [38], which suggest that the CB state gradually appears in our diagrams in place of the W state as the amplitude of the wrinkles increases, which translates into the increase of the substrate roughness A/λ for each λ. Moreover, an increasing strength of attraction between the droplet and the substrate favours the W state, in agreement with the theory [38]. While for very small amplitude ($A = 0.5\sigma$) the W state appears even for very small strength of attraction between the substrate and the droplet and the CB state is only partially present during the simulations, for $A > 0.5\sigma$, the CB state becomes stable and appears in
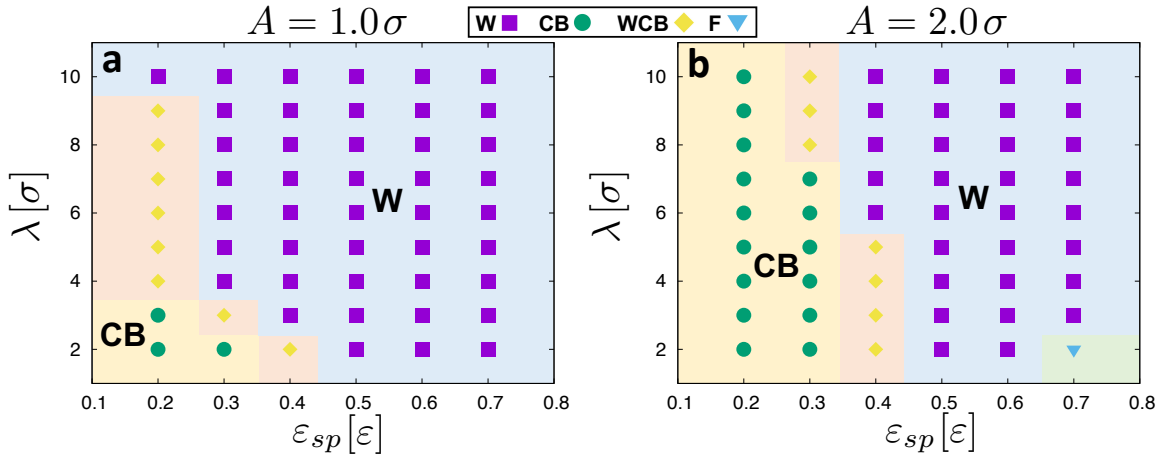
Fig. 2: State diagrams for droplets on wrinkled substrates without gradient as a function of the wavelength, λ, and the substrate–droplet attraction strength, ε_{sp}, for different substrate amplitudes, as indicated. Symbols are as follows: W: Wenzel state, CB: Cassie—Baxter state, WCB: droplet is in the W or the CB states at different instances in time during the simulation due to the thermal fluctuations, and F: Film (droplet spreading due to the strong attraction between the droplet and the substrate as the density of the wrinkles increases). Here, $N_p = 600$.

a larger number of cases as the roughness A/λ increases. However, the MD results also indicate the existence of a metastable state (WCB; Figure 2), where the droplet is either in the W or the CB state during the simulation. In addition, we observe that the WCB regime is generally narrow and, also, absent in particular cases as ε_{sp} increases. Our results can be summarised as follows: The formation of the W state is favoured by a small amplitude, A, a large wavelength, λ, and a large attraction between the droplet and the substrate, ε_{sp}. Our results are in agreement with the theoretical predictions and further comparisons with theory will be discussed in the following [38].

The equilibrium contact angle [**?**, 51–54], θ_E, provides the means of theoretically computing the free energies of Wenzel (W) and Cassie–Baxter (CB) states as a function of the substrate roughness $r = A/\lambda$ [38]. These results are presented in Fig. 3a for four representative values of θ_E. The free energies are given in dimensionless form, $F/(\gamma_{LV}\lambda\sigma)$, where γ_{LV} is the surface tension of the liquid–vapour boundary, and σ is the monomer diameter. As expected (Fig. 2a), with increasing roughness, the W state becomes metastable, while the CB state becomes stable. For each value of θ_E, this transition occurs at a particular critical roughness, A_c/λ. Above the line, the CB states are stable, while below the line the W states are stable. Following this analysis, the results obtained from the simulation are presented in Fig. 3b, which are in very good agreement with the theoretical predictions. In particular, for $\theta_E < 90°$, only W states are possible. In addition, as θ_E approaches 180°, even a small degree of roughness can induce the transition from W to CB states. The simulation results indicate that the boundary between the W and CB becomes sharper for larger values of θ_E. Finally, the CB state is absent for $\theta_E < 90°$ ($\varepsilon_{sp} > 0.6\varepsilon$), in agreement

with the theoretical calculations [38] (Fig. 3a). We have also analysed the different contributions to the free energy on the basis of a hybrid MD–DFT approach [46, 47] (See Supplmentary Information for more details on the method and references therein). In particular, we have identified the attractive term between the droplet and the substrate, F_{sp}, as the main factor that determines the state of the droplet (W or CB). Interestingly, the dependence of F_{sp} on the attraction strength, ε_{sp}, shows a faster than linear decrease as ε_{sp} increases, that is when the adhesion of the droplet to the substrate is stronger. This is due to the increase of the substrate density as the wrinkles become denser for smaller wavelengths, λ (inset of Fig. 3a). Moreover, differences in F_{sp} are small, at least for weaker adhesion, when the droplet is in 'loose' contact with the substrate.

We have analysed the rugotaxial motion for a wide and relevant range of parameters. From our results, we have determined that each case is distinct. For example, two substrates with the same gradient, G_λ, but different sets of (λ_0, λ_E) can show completely different behaviour regarding their ability to cause rugotaxial motion. Apart from these obvious differences, certain parameter combinations can cause the droplet to be in the W or CB states, the formation of a film, pinning, and others. In a recent molecular dynamics study [55], it has been found that even the slightest heterogeneity on the substrate can hinder the motion of a droplet on a substrate (pinning). Overcoming such a pinning barrier (depinning) can take place by an increasing interfacial energy between the droplet and the substrate as the droplet attempts to overcome the barrier, which can be achieved by exploiting changes of properties of the substrate along the direction of the motion. In this case, the difference in wettability along the pinning barrier has been exploited [55], while in our study the motion is
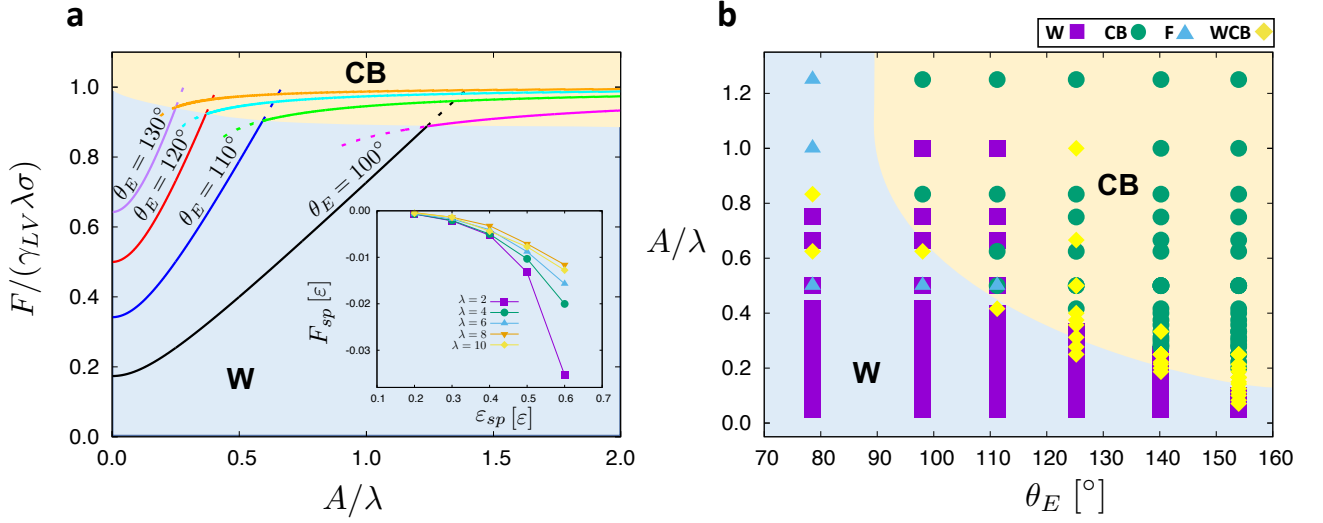
Fig. 3: (a) Free energies of Wenzel (W) and Cassie–Baxter (CB) states of a droplet with $N_p = 600$ as a function of substrate roughness, A/λ, for four values of the contact angle θ_E, as indicated. Solid lines correspond to stable states while dashed lines correspond to the metastable states. Inset presents the free energy component of the interaction between the droplet and the substrate as a function of the interaction parameter ε_{sp} for a substrate with $A = 2.0\sigma$. (b) Diagram of different states (W, CB, WCB, F) as a function of the roughness, A/λ, and the contact angle, θ_E (cf. Fig S1 of Supplementary Information showing the theoretical prediction [38]).

caused by the increasing density of the substrate along the rugotaxial motion due to the decrease of the wavelength, which in turn results in the increase of the interfacial energy between the droplet and the substrate. However, it is expected that CB and W states as well as pinning effects manifest differently along the substrate in the direction of the gradient, as it will be later discussed below. This further highlights that successful and efficient rugotaxis requires an appropriate design, which takes into account all these effects.

Based on our previous experience with investigations on the durotaxis phenomenon [17] and the experience gained by the current study, we have determined that the average rugotaxial velocity, V, of the droplet is an appropriate measure to assess the overall efficiency of the rugotaxis motion in successful cases, that is cases that can uninterruptedly translocate throughout the substrate in the direction of the wavelength gradient. In this case, $V = L/t$, where L is the distance covered by the centre of mass of the droplet during its translocation from the very left part of the substrate to the very right part of the substrate in the x direction (Fig. 1), and t is the time required to complete the rugotaxis motion. Then, Fig. 4 presents various characteristic examples that illustrate the dependence of the velocity for different droplet size and different scenarios of successful rugotaxis cases. In general, larger droplets are able to easier overcome the pinning barriers [55], with the latter becoming more pronounced as the droplet is in the Wenzel state (Fig. 2), which otherwise favour the rugotaxial motion. Still, one can observe the difference in the behaviour of large droplets ($N_p = 4800$) between substrates with $A = 0.5\sigma$ and $A = 2.0\sigma$, where the increase of ε_{sp} leads to different behaviour in the rugotaxis efficiency. Moreover, we have found that $A = 0.5\sigma$ leads to the most efficient rugotaxis, particularly for smaller droplets.

We take a closer look at the rugotaxis efficiency and inspect the different scenarios in our *in silico* experiments, providing, also, further insight into the parameters determining rugotaxis' performance (Fig. 4). We have identified a clear distinction between substrates with small ($A = 0.5\sigma$) and larger amplitudes $A > 0.5\sigma$. In particular, in the case of shallow wrinkles, $A = 0.5\sigma$, we observe two different scenarios. In the first scenario, the droplets attain their highest velocity V for small λ_0, namely $\lambda_0 = 2\sigma$ and $\lambda_E = \sigma$, albeit V tends to decrease with growing adhesion $\varepsilon_{sp} \gtrsim 0.4$. In particular, the motion of small droplets ($N_p = 100$) is significantly hampered as the adhesion strength ε_{sp} grows.

In contrast (cf. Fig. 4a), larger gradients (*e.g* $\lambda_0 = 6\sigma, \lambda_E = 3\sigma$), generally lower the mean velocity V which is found, however, to grow then steadily with increasing adhesion ε_{sp}. Moreover, the larger gradient ($\lambda_0 = 6\sigma, \lambda_E = 2\sigma$) nearly doubles V with respect to ($\lambda_0 = 6\sigma, \lambda_E = 3\sigma$) whereby for $\varepsilon_{sp} = 0.6$ the speed of the largest drop attains that from the first scenario. For deeper wrinkles, $A = 2\sigma$ (Fig. 4b), the same trend is observed although pinning effects occur more frequently so that for the case, $\lambda_0 = 2\sigma$, $\lambda_E = \sigma$ (not shown here), no rugotaxis whatsoever takes place. Apart from the smallest droplets, $N_p = 100$, an increase in the gradient G_λ leads similarly to faster motion, which becomes more efficient with growing drop size. However, further increase of the gradient or λ_0 will hinder
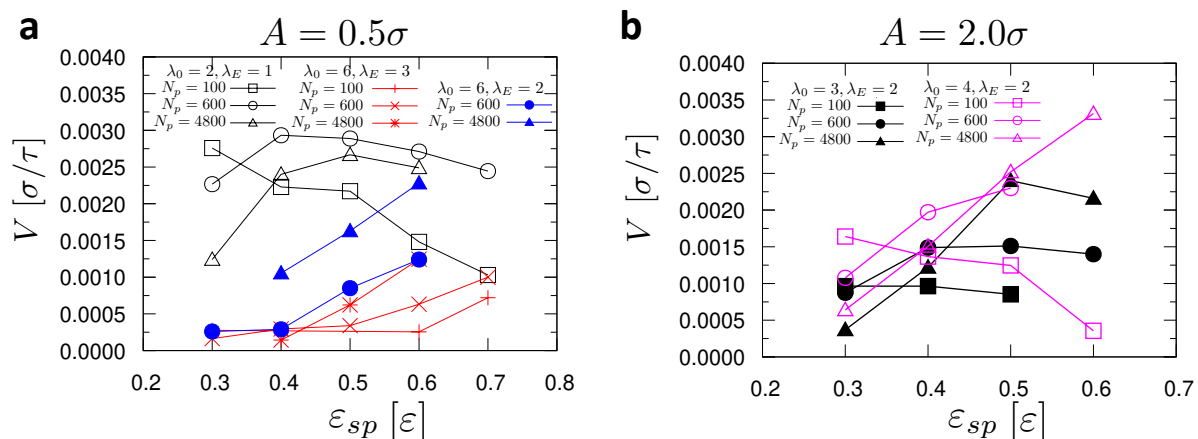
Fig. 4: The dependence of the average rugotaxis velocity, V, on the attraction strength, ε_{sp}, for different cases of λ_0, λ_E, N_p and A, as indicated.
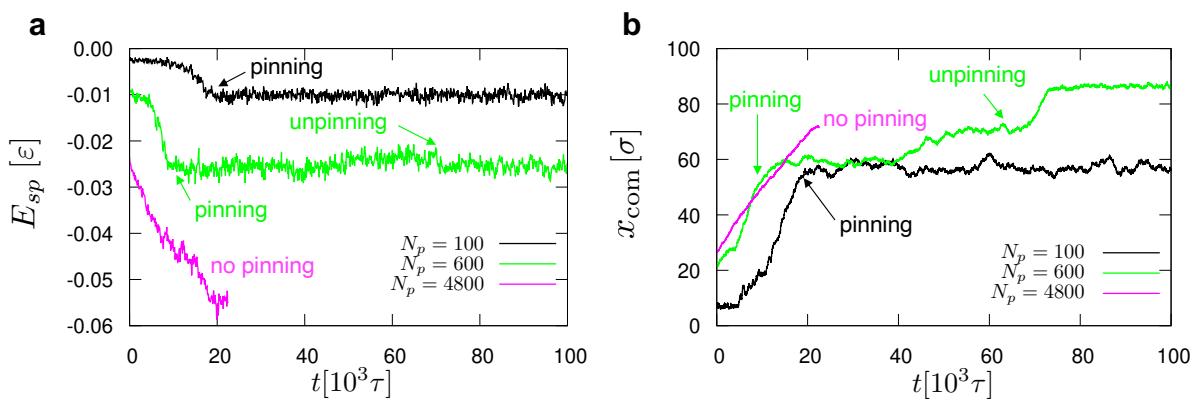

Fig. 5: Interfacial energy, E_{sp}, and position of the mass centre of the droplet, x_{com}, as a function of time, as indicated. Hence, the distance covered by the droplet refers to its centre of mass and droplets of different size will move a different distance in each *in silico* expriment. Arrows indicate the the time that pinning occurs for different cases of N_p as indicated. We also indicate the unpinning of the droplet with an arrow in the case of $N_p = 600$. For $N_p = 100$, the droplet remains pinned throughout the simulation. For $N_p = 4800$, there is no pinning. Here, $A = 2$, $\lambda_0 = 4\sigma$, $\lambda_E = \sigma$, $\varepsilon_{sp} = 0.4\varepsilon$. $N_p = 100$, 600 and 4800, as indicated.

the motion of the droplets, independently of the droplet size. Moreover values of $\varepsilon_{sp} = 0.7\varepsilon$ (strong adhesion of the droplet to the substrate) will always prevent the motion of the droplet or lead to complete droplet spreading (*e.g.* for $N_p = 4800$). Still, we have observed that larger droplets overcome more easily the pinning barriers, which is in agreement with recent simulation results [55].

As in the case of durotaxial motion [17], we have identified the change in the interfacial energy between the droplet and the substrate as the main driving force of rugotaxis, also determining its efficiency (Fig. 5). In our case, the interfacial energy is simply the total pair interaction between the droplet and the substrate beads. Crucially, for a certain droplet size this depends on the particular parameters, A, ε_{sp}, λ_0, and λ_E. We have also identified cases when the droplet exhibits pinning during rugotaxis but is also able to overcome the associated energy bar-

rier caused by the pinning and eventually complete the rugotaxial motion. While in such cases, rugotaxis is successful and eventually the droplet reaches the very right end of the substrate (Fig. 5), in many other cases considered in our study as unsuccessful rugotaxis cases, the droplet failed to overcome the associated energy barrier. Typically, such pinning events occur at the transition from W- to CB-state as the drop partially climbs out of the substrate troughs whereby the interfacial energy E_{sp} rises before the *whole* droplet attains a new CB-state where droplet beads cannot enter into the narrowed wrinkles [55].

Figure 5 contains plots of the position of the centre of mass of the droplet, x_{com}, and the interfacial energy, E_{sp}, as a function of the elapsed time from the beginning until the end of the rugotaxial motion. For $N_p = 600$, we find that the droplet tranlocates efficiently until pinning occurs. An important point here is that the energy, E_{sp},

continues to decrease just after the pinning, which allows the droplet to move to the right, where the underlying density and wettability of the substrate increases with the wavelength gradient.

In summary, we have investigated solid, wrinkled substrates with and without wavelength gradient in one direction, in an attempt to explore the rugotaxial motion of droplets. To achieve our goal we have mainly employed MD simulation based on coarse-grained force-fields, as we have done previously in the case of durotaxis. [17] We have also provided relevant theoretical background and, also, performed numerical calculations based on a hybrid MD–DFT approach. [46,47,56]

We have constructed the diagram of W and CB states for a range of parameters. For small wrinkle amplitudes, the W state prevails for a range of droplet–substrate adhesion strength and wrinkle wavelengths. As the amplitude increases, the CB state sets in initially at small adhesion strengths and wrinkle wavelengths. As the amplitude further increases, the CB state appears for a larger range of wavelengths and adhesion strengths. Theory [38] predicts the boundary between W and CB states, which is in agreement with the simulation results. Based on a hybrid MD–DFT approach, we have identified the interfacial energy-term to be mainly responsible for the different behaviour (W or CB).

In the case of the rugotaxis MD *in silico* experiments, we find a range of optimal choices of the parameters that govern rugotaxis. In the case of shallow wrinkles with $A = 0.5\sigma$, we observe the most efficient rugotaxial motion for $\lambda_0 = 2\sigma$, which corresponds to a small wavelength gradient. For larger amplitudes, increased wavelength gradients lead to more efficient rugotaxis up to some moderate adhesion strength. As a result, our results indicate that an appropriate substrate design will determine the efficiency of the rugotaxial motion.

Based on our analysis, we have identified that changes of the interfacial energy between the substrate and the droplet constitute the driving force of rugotaxial motion, as has been also found previously in the case of durotaxis. [17] Hence, the two phenomena share characteristics, but, in the case of rugotaxis, this crucially depends on a larger number of parameters that can lead to different scenarios with pinning playing a crucial role. We anticipate that our study elucidates important aspects of the rugotaxis phenomenon and suggests design principles for nano-fabricated wirnkle-patterned substrates that can increase the efficiency of rugotaxial motion.

$* * *$

REFERENCES

[1] M. Srinivasarao, D. Collings, A. Philips, and S. Patel. Three-dimensionally ordered array of air bubbles in a polymer film. Science, 292:79–83, 2001.

[2] Manoj K. Chaudhury and George M. Whitesides. How to make water run uphill. Science, 256(5063):1539–1541, 1992.

[3] T.-S. Wong, S. H. Kang, S. K. Y. Tang, E. J. Smythe, B. D. Hatton, A. Grinthal, and J. Aizenberg. Bioinspired self-repairing slippery surfaces with pressure-stable omniphobicity. Nature, 477:443–447, 2011.

[4] G. Lagubeau, M. Le Merrer, C. Clanet, and D. Quéré. Leidenfrost on a ratchet. Nat. Phys., 7:395–398, 2011.

[5] M. Prakash, D. Quéré, and J. W. Bush. Surface tension transport of prey by feeding shorebirds: The capillary ratchet. Science, 320:931–934, 2008.

[6] A. Darhuber and S. Troian. Principles of microfluidic actuation by modulation of surface stresses. Annu. Rev. Fluid Mech., 37:425–455, 2005.

[7] Z. Yao and M. J. Bowick. Self-propulsion of droplets by spatially-varying surface topography. Soft Matter, 8(4):1142–1145, 2012.

[8] H. Li, T. Yan, K. A. Fichthorn, and S. Yu. Dynamic contact angles and mechanisms of motion of water droplets moving on nano-pillared superhydrophobic surfaces: A molecular dynamics simulation study. Langmuir, 34:9917–9926, 2018.

[9] A. Bardall, S.-Y. Chen, K. E. Daniels, and M. Shearer. Gradient-induced droplet motion over soft solids. IMA Journal of Applied Mathematics (Institute of Mathematics and Its Applications), 85(3):495–512, 2020.

[10] G. Karapetsas, N. T. Chamakos, and A. G. Papathanasiou. Efficient modelling of droplet dynamics on complex surfaces. J. Phys.: Condens. Matter, 28(8):085101, 2016.

[11] B. Zhang, X. Liao, Y. Chen, H. Xiao, Y. Ni, and X. Chen. Rapid Programmable Nanodroplet Motion on a Strain-Gradient Surface. Langmuir, 35(7):2865–2870, 2019.

[12] J. Leng, Y. Hu, and T. Chang. Nanoscale directional motion by angustotaxis. Nanoscale, 12:5308–5312, 2020.

[13] K. A. Lazopoulos and D. Stamenović. Durotaxis as an elastic stability phenomenon. J. Biomech., 41(6):1289–1294, 2008.

[14] I. Palaia, A. Paraschiv, V. E. Debets, C. Storm, and Anđela Šarić. Durotaxis of passive nanoparticles on elastic membranes. ACS Nano, 0(0):null, 0.

[15] A. S. Barnard. Nanoscale locomotion without fuel. Nature, 519:37–38, 2015.

[16] T. Chang, H. Zhang, Z. Guo, X. Guo, and H. Gao. Nanoscale directional motion towards regions of stiffness. Phys. Rev. Lett., 114(1):015504, 2015.

[17] P. E. Theodorakis, S. A. Egorov, and A. Milchev. Stiffness-guided motion of a droplet on a solid substrate. J. Chem. Phys., 146(24):244705, 2017.

[18] M. Becton and X. Wang. Controlling nanoflake motion using stiffness gradients on hexagonal boron nitride. RSC Adv., 6:51205–51210, 2016.

[19] M. Becton and X. Wang. Thermal gradients on graphene to drive nanoflake motion. J. Chem. Theory Comput., 10:722–730, 2014.

[20] F.D. Dos Santos; and Thierry Ondarquhus. Free-Running Droplets Fabrice. Physcal Review Letters, 75(16):2972, 1995.

[21] Seok Won Lee, Daniel Y. Kwok, and Paul E. Laibinis. Chemical influences on adsorption-mediated self-propelled drop movement. Physical Review E - Statistical Physics, Plasmas, Fluids, and Related Interdisciplinary Topics, 65(5):9, 2002.

[22] Susan Daniel and Manoj K Chaudhury. ( ) (4) (1). (8):3404–3407, 2002.

[23] P. Brunet, J. Eggers, and R. D. Deegan. Vibration-induced climbing of drops. Physical Review Letters, 99(14):3–6, 2007.

[24] Philippe Brunet, J. Eggers, and R. D. Deegan. Motion of a drop driven by substrate vibrations. European Physical Journal: Special Topics, 166(1):11–14, 2009.

[25] A. Buguin, L. Talini, and P. Silberzan. Ratchet-like topological structures for the control of microdrops. Applied Physics A: Materials Science and Processing, 75(2):207–212, 2002.

[26] Uwe Thiele and Karin John. Transport of free surface liquid films and drops by external ratchets and self-ratcheting mechanisms. Chemical Physics, 375(2-3):578–586, 2010.

[27] Xavier Noblin, Richard Kofman, and Franck Celestini. Ratchetlike motion of a shaken drop. Physical Review Letters, 102(19):1–4, 2009.

[28] S. Hiltl and A. Böker. Wetting Phenomena on (Gradient) Wrinkle Substrates. Langmuir, 32(35):8882–8888, 2016.

[29] F. Brochard. Motions of droplets on solid surfaces induced by chemical or thermal gradients. Langmuir, 5(2):432–438, 1989.

[30] Len M. Pismen and Uwe Thiele. Asymptotic theory for a moving droplet driven by a wettability gradient. Physics of Fluids, 18(4), 2006.

[31] E. Cerda and L. Mahadevan. Geometry and physics of wrinkling. Phys. Rev. Lett., 90:074302, 2003.

[32] A. Malijevský. Filling, depinning, unbinding: Three adsorption regimes for nanocorrugated substrates. Phys. Rev. E, 012804:1–13, 2020.

[33] S. Hiltl, M.-P. Schürings, A. Balaceanu, V. Mayorga, C. Liedel, A. Pich, and A. Böker. Guided self-assembly of microgels: from particle arrays to anisotropic nanostructures. Soft Matter, 7:8231–8238, 2011.

[34] S. G. Lee, H. S. Lim, D. Y. Lee, D. Kwak, and K. Cho. Tunable anisotropic wettability of rice leaf-like wavy surfaces. Adv. Funct. Mater., 23(5):547–553, 2013.

[35] K. W. Sun, M. S. Ambrosia, T. W. Kwon, and M. Y. Ha. A hydrophobicity study on wavy and orthogonal textured surfaces. Computers and Fluids, 140:347–356, 2016.

[36] J. Y. Chung, A. J. Nolte, and C. M. Stafford. Surface wrinkling: A versatile platform for measuring thin-film properties. Adv. Mater., 23:349–368, 2011.

[37] H. E. Jeong, M. K. Kwak, and K. Y. Suh. Stretchable, adhesion-tunable dry adhesive by surface wrinkling. Langmuir, 26:2223–2226, 2010.

[38] G. Carbone and L. Mangialardi. Hydrophobic properties of a wavy rough substrate. Eur. Phys. J. E, 16(1):67–76, 2005.

[39] J. A. Ko, M. Ambrosia, and M. Y. Ha. A study of the wetting characteristics of a nano-sized water droplet on heterogeneous striped surfaces. Comput. Fluids, 112:19–34, 2015.

[40] Matthew Stanley Ambrosia, Joonkyung Jang, and Man Yeong Ha. Static and dynamic hydrophobicity on a nano-sized groove/ridge surface. Comput. Fluids, 114:75–83, 2015.

[41] D. M. Spori, T. Drobek, S. Zürcher, M. Ochsner, C. Sprecher, A. Mühlebach, and N. D. Spencer. Beyond the lotus effect: Roughness influences on wetting over a wide surface-energy range. Langmuir, 24(10):5411–5417, 2008.

[42] V. Kumar and J. R. Errington. Impact of small-scale geometric roughness on wetting behavior. Langmuir, 29(38):11815–11820, 2013.

[43] E. M. Grzelak and J. R. Errington. Nanoscale limit to the applicability of Wenzel's equation. Langmuir, 26(16):13297–13304, 2010.

[44] C. Liu, I. Legchenkova, L. Han, W. Ge, C. Lv, S. Feng, E. Bormashenko, and Y. Liu. Directional droplet transport mediated by circular groove arrays. part i: Experimental findings. Langmuir, 36(32):9608–9615, 2020.

[45] C. Liu, I. Legchenkova, L. Han, W. Ge, C. Lv, S. Feng, E. Bormashenko, and Y. Liu. Directional droplet transport mediated by circular groove arrays. part ii: Theory of effect. Langmuir, 37(5):1948–1953, 2021.

[46] F. Lo Verso, L. Yelash, S.A. Egorov, and K. Binder. Interactions between polymer brush-coated spherical nanoparticles: The good solvent case. J. Chem. Phys., 135:214902, 2011.

[47] A. Milchev, S.A. Egorov, D.A. Vega, K. Binder, and A. Nikoubashman. Densely packed semiflexible macromolecules in a rigid spherical capsule. Macromolecules, 51:2002–2016, 2018.

[48] A. B. D. Cassie and S. Baxter. Wettability of porous surfaces. Trans. Faraday Soc., (5):546–551, 1944.

[49] R. N. Wenzel. Resistance of solid surfaces to wetting by water. Ind. Eng. Chem. Res., 28(8):988–994, 1936.

[50] W. Humphrey, A. Dalke, and K. Schulten. VMD: Visual Molecular Dynamics. J. Mol. graph., 14:33–38, 1996.

[51] P.-G. de Gennes, F. Brochard-Wyart, and D. Quéré. Capillarity and wetting phenomena: Drops, bubbles, pearls, waves. Springer, New York, 2004.

[52] P. G. De Gennes. Wetting: Statics and dynamics. Reviews of Modern Physics, 57(3):827–863, 1985.

[53] P. E. Theodorakis, E. A. Müller, R. V. Craster, and O. K. Matar. Modelling the superspreading of surfactant-laden droplets with computer simulation. Soft Matter, 11:9254–9261, 2015.

[54] E. R. Smith, P. E. Theodorakis, R. V. Craster, and O. K. Matar. Moving contact lines: Linking molecular dynamics and continuum-scale modeling. Langmuir, 34:12501–12518, 2018.

[55] P. E. Theodorakis, A. Amirfazli, B. Hu, and Z. Che. Droplet control based on pinning and substrate wettability. Langmuir, 37(14):4248–4255, 2021.

[56] H. Xu, L. HongLai, and H. Ying. Dynamic density functional theory based on equation of state. Chem. Eng. Sci., 62:3494–2016, 2007.